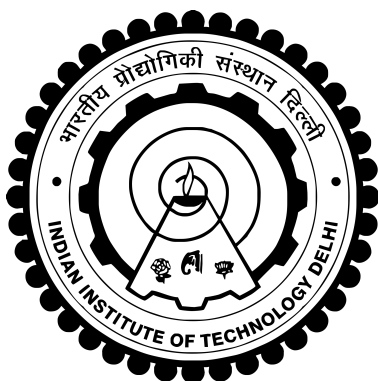


**CONTROLLING OF PV INTEGRATED GRID-TIED CONVERTERS:
REDUCED DC-LINK CAPACITOR AND REDUCED SENSORS**

KHUSHBOO KUMARI



**DEPARTMENT OF ELECTRICAL ENGINEERING
INDIAN INSTITUTE OF TECHNOLOGY DELHI
FEBRUARY 2024**

© Indian Institute of Technology Delhi (IITD), NewDelhi, 2024

CONTROLLING OF PV INTEGRATED GRID-TIED CONVERTERS: REDUCED DC-LINK CAPACITOR AND REDUCED SENSORS

A THESIS

submitted by

KHUSHBOO KUMARI

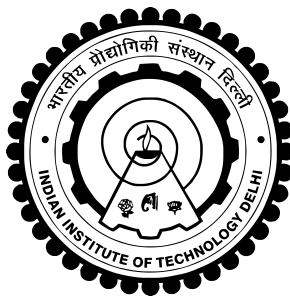
under the supervision of

Prof. Amit Kumar Jain

in fulfillment of the requirements of the degree

of

Doctor of Philosophy



**Department of Electrical Engineering
INDIAN INSTITUTE OF TECHNOLOGY DELHI**

FEBRUARY 2024

Certificate

This is to certify that the thesis titled “**CONTROLLING OF PV INTEGRATED GRID-TIED CONVERTERS: REDUCED DC-LINK CAPACITOR AND REDUCED SENSORS**”, submitted by **Khushboo Kumari**, for the award of the degree of **Doctor of Philosophy** in the Department of Electrical Engineering, Indian Institute of Technology, Delhi, is a bonafide record of the research work done by her under my supervision. The contents of this thesis, in full or in parts, have not been submitted to any other Institute or University for the award of any degree or diploma.

Dated:

(Dr. Amit Kumar Jain)

**Department of Electrical Engineering
Indian Institute of Technology, Delhi
Hauz khas, New Delhi-110016, India**

Acknowledgements

It is my pleasure to remind and acknowledge the outstanding individuals, who in one way or another provided stupendous support in the completion of my doctoral research. This thesis would not have been possible without the guidance and assistance of such extraordinary persons.

First of all, I would like to express my special thanks of gratitude to **Prof. Amit Kumar Jain**, my thesis supervisor, for continuous support and for taking me through thick and thin during the course of my research journey. I always admire his patience and calm stature. His insight and discernment have led me to get the maximum in my research area. The consequence of persistent brainstorming sessions with him has yielded several ideas that have helped me to complete my research work. He is truly an extraordinary advisor who has extended his help in my doctoral research and offered significant support in balancing my professional and personal life.

Second, I would like to thank my review committee members, **Prof. M. Veerachary**, **Dr. Anandarup Das**, and **Dr. Ashu Verma**, for constantly supervising, providing suggestions, and thoughtfulness through research progress sessions which have led me to improvise and refine my research work. I would like to thank **Prof. Amit Kumar Jain** and **Dr. Anandarup Das** for providing an excellent research environment and laboratory facilities. I also like to thank **Mr. Sumit Kumar Singh**, **Mr. Dhanraj Singh**, and late **Mr. Suresh Chand** for assisting in procuring items for the experimental setup.

I would also like to express my sincere thanks to my seniors, peers, and colleagues for constantly getting involved in technical discussions. I would like to especially thank **Miss Cheshta Jain** for supporting me emotionally and spiritually during tough times. I would also like to acknowledge the efforts of my seniors **Dr. Prasun Mishra**, **Dr. Kapil Shukla**, and **Dr. Nikhil Krishna Bajjuri** to uplift my motivation and encourage me while implementing my experimental setup. I will always cherish **Mr. Navneet Vaishnav** for having technical discussions on the control aspect. I would also like to thank **Mr. Rahul Sharma** and **Mrs. Nidhi Bist** for constantly helping me in my personal as well as professional life. I would also send my best wishes and thanks to all the lab-mates, **Mr. Martin Cheerangal**, **Mr. Aamir Rafiq**, and **Miss Apurva Verma**.

Lastly, I revere my parents and all my family members for constantly motivating, encouraging, and supporting me through my research journey. Especially, I would like to express my sincere gratitude to my husband for being patient and calm during the course of my research work.

A small, square image showing a handwritten signature in blue ink that reads "Khushboo".

(Khushboo Kumari)

Abstract

This thesis deals with the analysis, modeling, simulation, and implementation of solar photovoltaic (PV) integrated grid-tied neutral point clamped (NPC) converters. The converter is interfaced with the grid through an *LCL* filter, which introduces resonance in the grid current. The resonance in the grid current leads to instability in the system. This thesis contributes to the control aspect, minimization of complexity, and increases reliability and harmonic content in the implementation.

Extensive loss analysis is carried out between NPC and T-Type three-level converter for different semiconductor devices based on Si, SiC, and GaN comprehensively. This facilitates the selection of the best three-level converter for the grid-tied converter. The three-level NPC is chosen for interfacing solar PV to the grid. To meet the demand for reduction in cost and weight and also increase in reliability of the *LCL* filter-based grid-tied converter, a cascaded control for the *LCL* filter-based grid-connected NPC inverter with the reduced sensor is proposed and incorporated in the thesis. Multiple loop control strategies are generally preferred to achieve better system stability. However, the multiple loop control technique utilizes numerous sensors, which increases weight, and cost and decreases the system's reliability. A novel cascaded control scheme that considerably reduces grid-side current and capacitor-side voltage sensors is implemented. Only two inverter-side current sensors are required. The proposed estimation algorithm implements the sensing point. Estimating the grid-side current and the capacitor voltage is carried out through the sensed inverter side current. Another less sensor-based scheme is proposed in this thesis that is based on sensing capacitor side voltage for the *LCL* filter-based grid-connected NPC inverter.

The robust and stable control technique utilizing less number of sensors is a significant concern in *LCL* filter-based grid-connected converter for the weak grid that requires considerable research attention. This thesis incorporates a Trilateral control scheme for *LCL* filter-based system with a single grid current sensor in the weak grid. This work implements a novel control scheme utilizing a single sensor to sense the grid current. This technique has reduced a considerable number of current sensors and voltage sensors. The α axis of the grid current is proportional to the sensed 'a' phase grid current. The β current in the utility grid is acquired by employing the controller reference quantities of the grid current. The computation of another variable, *i.e.*, the current in the inverter side inductor and the voltage across the capacitor, is executed by an estimation algorithm. The proposed technique provides the feature of reducing implementation financial value and weight and reduces the complexity and size of hardware.

In order to enhance the reliability, lifetime expectancy, improved efficiency, and reduced cost of the system, an effective reduction in the capacitor size of the DC-bus of a conventional three-phase NPC inverter-based grid-integrated single-stage solar photovoltaic (PV) system is also integrated into the thesis. It also retains the feature of minimal oscillations during the change in irradiation.

A twelve insulated gate bipolar transistor (K40H603) with their appropriate drivers and six diodes (FFPF30UA60S) based experimental set-up is developed in the laboratory. Texas instruments-based DSP TMS320F28335 digital controller is utilized to run the set-up. The system performance is observed using a MATLAB version simulation model and authenticated through the experimental results obtained from the laboratory prototype.

सारांश

यह थीसिस सौर फोटोवॉल्टेक (PV) इंटीग्रेटेड ग्रिड-टाइड न्यूट्रल पॉइंट क्लैम्प (NPC) कनवर्टर के विश्लेषण, मॉडलिंग, सिमुलेशन, और अमलीकरण के साथ संबंधित है। कनवर्टर ग्रिड से LCL फिल्टर के माध्यम से इंटरफेस है, जो ग्रिड के वर्तमान में रीसोनेंस लाता है। ग्रिड के वर्तमान में रीसोनेंस सिस्टम में अस्थिरता की ओर ले जाता है। यह थीसिस नियंत्रण पहलू, जटिलता की कमी, और अमलीकरण में सत्ता और हार्मोनिक सामग्री को कम करने में योगदान करती है।

एनपीसी और टी-टाइप तीन स्तरीय कनवर्टर के बीच व्यापक हानि विश्लेषण प्रदर्शित किया गया है जो विभिन्न सिलिकॉन, एसआईसी, और गैन पर आधारित अलग-अलग अर्धचालक उपकरणों के लिए होता है। यह सूर्य PV को ग्रिड से इंटरफेस करने के लिए तीन स्तरीय एनपीसी का चयन करता है। लागत और वजन में कमी और सुरक्षा में वृद्धि के लिए एलसीएल फिल्टर आधारित ग्रिड-टाइड कनवर्टर के लिए एक कास्केड नियंत्रण प्रस्तावित किया गया है और थीसिस में शामिल किया गया है। मल्टीपल लूप नियंत्रण रणनीतियों को सामान्यतः बेहतर सिस्टम स्थिरता प्राप्त करने के लिए पसंद किया जाता है। हालांकि, मल्टीपल लूप नियंत्रण तकनीक कई सेंसरों का उपयोग करती है, जो वजन और लागत बढ़ाता है और सिस्टम की सुरक्षा को कम करता है। एक नवीन कास्केड नियंत्रण योजना जो ग्रिड साइड करंट और कैपेसिटर साइड वोल्टेज सेंसर को कम करने के लिए काफी अच्छा है, प्रस्तावित किया जाता है। केवल दो इन्वर्टर-साइड करंट सेंसर की आवश्यकता है। प्रस्तावित अनुमान एल्गोरिदम सेंसिंग प्वाइंट को लागू करता है। ग्रिड-साइड करंट और कैपेसिटर वोल्टेज का अनुमान इन्वर्टर साइड करंट के माध्यम से किया जाता है। एक और कम सेंसर-आधारित योजना को इस थीसिस में प्रस्तावित किया गया है जो LCL फिल्टर आधारित ग्रिड-टाइड NPC इन्वर्टर के लिए कैपेसिटर साइड वोल्टेज

सुदृढ़ और स्थिर नियंत्रण तकनीक जो कम संख्या में सेंसर का उपयोग करती है, वे दुर्बल ग्रिड के लिए LCL फिल्टर आधारित ग्रिड-कनेक्टेड कनवर्टर में महत्वपूर्ण चिंता है जो विशेष रूप से अध्ययन की जरूरत है। यह थीसिस LCL फिल्टर आधारित प्रणाली के लिए एक त्रिकोणीय नियंत्रण योजना को शामिल करती है जिसमें एक ही ग्रिड करंट सेंसर का उपयोग दुर्बल ग्रिड में किया जाता है। यह काम ग्रिड करंट को महसूस करने के लिए एक ही सेंसर का उपयोग करने वाली एक नई नियंत्रण योजना को लागू करता है। इस तकनीक ने एक बड़ी संख्या की सेंसर और वोल्टेज सेंसर को कम किया है। ग्रिड करंट का α धुरी जो 'a' चरण ग्रिड करंट को महसूस करने के लिए है, यह β करंट उपयोग करता है जो सेंसर करंट कंट्रोलर संदर्भ मात्राओं का उपयोग करके उपयोगिता ग्रिड में है। एक अन्य परिवर्तन, अर्थात् इन्वर्टर साइड इंडक्टर में करंट और कैपेसिटर के वोल्टेज की गणना एक अनुमान एल्गोरिथम के द्वारा की जाती है। प्रस्तावित तकनीक को अमलीकरण वित्तीय मूल्य और वजन को कम करने की सुविधा प्रदान करती है और हार्डवेयर की जटिलता और आकार को कम करती है।

सिस्टम की विश्वसनीयता, जीवनकाल अपेक्षा, बेहतर कुशलता, और कम लागत को बढ़ावा देने के लिए, एक पारंपरिक तीन-चरण NPC इन्वर्टर आधारित ग्रिड-इंटीग्रेटेड एक-मंजिल सौर फोटोवॉल्टेक (PV) सिस्टम के DC-बस के कैपेसिटर के आकार में प्रभावी कमी भी थीसिस में शामिल की गई है। यह भी इसकी विशेषता को बनाए रखता है कि प्रकाश संचार में परिवर्तन के दौरान न्यूनतम अदल-बदल होता है।

एक बारह इंसुलेटेड गेट बायपॉलर ट्रांजिस्टर (K40H603) के साथ उनके उपयुक्त ड्राइवर और छह डायोड (FFPF30UA60S) पर आधारित प्रयोगशाला सेट-अप विकसित किया गया है। टेक्सास इंस्ट्रूमेंट्स आधारित DSP TMS320F28335 डिजिटल नियंत्रक का उपयोग सेट-अप को चलाने के लिए किया गया है। सिस्टम के प्रदर्शन को एक MATLAB संस्करण सिमुलेशन मॉडल का उपयोग करके देखा गया है और प्रयोगशाला प्रोटोटाइप से प्राप्त प्रयोगात्मक परिणामों के माध्यम से प्रमाणित किया गया है।

Contents

CERTIFICATE	i
ACKNOWLEDGEMENTS	ii
ABSTRACT	iv
सारांश	vi
LIST OF FIGURES	xx
LIST OF TABLES	xxi
ABBREVIATIONS	xxiii
NOMENCLATURE	xxv
1 Introduction	1
1.1 Power Electronic Interfaces: Overview	1
1.2 Harmonic Filters in Power Electronic Converters for Grid Integration . . .	4
1.3 Comparative Analysis of Active Damping: Single-Loop vs. Multiple-Loop Control	7
1.4 Literature on Control of Grid Connected Converter	10
1.4.1 Literature on Control of the System with Single Grid Current Sensor	14
1.4.2 Literature on Control of the System with Single Grid Current Sensor in Weak Grid	16
1.5 Literature on Phase Locked loop	17
1.6 Literature on Reduction of the Capacitor of Grid Connected System . . .	20
1.7 Objectives and Scope of the Work	21
1.8 Outline of Thesis	22
2 Design, Modelling, and Control of Grid Connected Converter	25

2.1	Design of <i>LCL</i> Filter for Grid Connected Converter	25
2.2	Modelling of Grid Connected Converter	33
2.3	Control of Grid Connected Converter	37
2.3.1	Inner Loop Control	37
2.3.2	Middle Loop Control	42
2.3.3	Outer Loop Control	45
2.3.4	DC-bus Voltage Control Loop	47
2.3.5	Controller for MPPT loop	48
2.4	Reference Derivation	48
2.4.1	Reference Derivation for Middle loop	48
2.4.2	Reference Derivation for Inner loop	49
2.5	Design of Controller Parameters	49
2.5.1	Inner Loop Control Parameters	51
2.5.2	Middle Loop Control Parameters	52
2.5.3	Outer Loop Control Parameters	52
2.6	Conclusion	53
3	Control of <i>LCL</i> Filter Based Grid Connected Converter Based on Esti- mation Algorithm for Reduced Sensor	55
3.1	Cascaded Control Scheme Based on Sensing Inverter Current	56
3.2	Cascaded Control Scheme Based on Sensing Capacitor Voltage	61
3.3	Analysis of Proposed Control	64
3.3.1	Variation in Impedance of the Utility Grid	64
3.3.2	Effect of the Parameter Variation on the System Stability	64
3.3.3	Effect of the Variation in Delay Time T_d on the System Stability	66
3.3.4	Observability	67
3.3.5	Comparison of the Scheme	71
3.4	Cascaded Control Scheme Based on Single Current Sensor	71
3.4.1	Schematic of the System	73
3.4.2	Three Loop Control Technique Based on Grid Current Measurement	74
3.4.3	Algorithm of State Variables Based on Sensing Grid Side Inductor Current	75

3.4.4	Algorithm for Computing Grid Side Inductor Current in β axis . . .	78
3.5	Results and Discussions	80
3.5.1	Simulation Results	80
3.5.2	Experimental Results	87
3.6	Conclusion	93
4	Control of <i>LCL</i> Filter Based Grid Connected Converter Based on Estimation Algorithm for Reduced Sensor in Weak Grid and Discrete SOGI Controller for Solar Photovoltaic System	95
4.1	Proposed Estimation Algorithm Based on Reduced Sensor in Weak Grid Conditions	96
4.1.1	Control Technique	99
4.1.2	Decoupled Grid Voltage and Decoupled Grid Current	112
4.1.3	Mathematical Characterization of the Converter in the Presence of Unbalanced Conditions	115
4.1.4	Philosophy for Single Current Sensor	121
4.2	IIR Digital Filter Based Discrete SOGI Controller and Discrete DSOGI PLL for Grid Integrated Solar Photovoltaic System	122
4.2.1	Control Strategies	123
4.3	Results and Discussions	134
4.3.1	Simulation Results	134
4.3.2	Experimental Results	140
4.4	Conclusion	142
5	Grid Integrated Solar PV System with Reduced DC-bus Capacitor	145
5.1	Design of the Inverter	147
5.2	Lifetime, Reliability, and Cost	148
5.2.1	Lifetime	148
5.2.2	Reliability	152
5.2.3	Cost	153
5.3	PWM Technique Implemented in the System	156
5.4	Control Methodology	159
5.4.1	Neutral Point Voltage Dynamics and Voltage Balancing Control for DC-bus Capacitor	160

5.4.2	Controller for Current Loop	162
5.4.3	Controller for MPPT Loop	163
5.5	Results and Discussions	164
5.5.1	Simulation Result	164
5.5.2	Experimental Result	165
5.6	Conclusion	170
6	Conclusions and Future Scope	172
6.1	General	172
6.2	Major Conclusions	172
6.3	Summary of Present Work and Key Contributions	173
6.3.1	Key Contributions of Chapter 2	174
6.3.2	Key Contributions of Chapter 3	174
6.3.3	Key Contributions of Chapter 4	175
6.3.4	Key Contributions of Chapter 5	175
6.4	Future Scope	176
A	Loss Analysis of NPC and T-Type Three-Level Converter for Si, SiC, and GaN-Based Devices	179
A.1	Equation of Conduction and Switching losses	182
A.1.1	Conduction and Switching Losses in NPC Converter	182
A.1.2	Conduction and Switching Losses in T-type Converter	183
A.2	Analysis	183
A.3	Discussions	186
B	Experimental Set-up	189
B.1	Inverter	189
B.1.1	Gate Driver Board	190
B.1.2	Power Board	190
B.1.3	Sensor Circuit	190
B.2	PCB Design	191
C	Parameters	193

C.1	System Parameter	193
C.1.1	Parameter in Simulation	193
C.1.2	Parameter in Experimental	193
C.2	Controller Parameter in Chapter 3	194
C.3	Parameter in Chapter 4	194
C.4	Parameter in Chapter 5	195
	References	196
	Bio-data and List of Publications/Patents	205

List of Figures

1.1	Voltage source inverter.	2
1.2	NPC inverter.	2
1.3	CHB multilevel inverter.	3
1.4	System with L filter.	5
1.5	System with LCL filter.	6
1.6	Single-loop control technique.	7
1.7	Multiple-loop control technique.	8
1.8	Grid integrated single stage solar PV system with NPC converter.	9
1.9	Undamped single-phase circuit.	10
1.10	Single-phase circuit with a damping resistor in series.	10
1.11	Diagram illustrating control based on active damping utilizing a virtual resistor with k_r	10
1.12	Diagram illustrating control based on active damping utilizing a virtual resistor with k_c	11
1.13	Control block of 3-loop control for LCL filter in $d-q$ synchronous reference frame.	12
1.14	Control structure diagram of the i_C internal-loop feedback.	13
1.15	Closed loop control system structure of three-phase VSI.	14
1.16	Control block diagram of LCL filter based grid-integrated converter based on full-order observer.	15
1.17	Control block diagram of LCL filter based grid-integrated converter based on reduced order observer.	16
1.18	Generalized structure of PLL.	18
1.19	Block diagram of SOGI.	18
1.20	Block diagram of a modified SOGI.	19
1.21	Block diagram of a MNF SOGI.	19
2.1	Schematic diagram of grid-tied converter with LCL filter.	26
2.2	Single-phase equivalent circuit.	26

2.3	Single-phase circuit of LCL filter.	27
2.4	Block diagram of LCL filter.	27
2.5	Bode plot of $i_g(s)/v_i(s)$ for different passive elements given in Table 2.2.	30
2.6	Design flow for the LCL -filter where Y corresponds to Yes, N corresponds to No.	32
2.7	Single-phase equivalent circuit.	33
2.8	Block diagram of cascaded control with decoupling unit.	36
2.9	Control block of cascaded control with feedforward compensation.	37
2.10	Control block of cascaded control system in d -axis.	38
2.11	Block diagram of cascaded control for LCL filter in d - q coordinate system with an estimated algorithm based on sensing inverter side inductor current.	39
2.12	Block diagram of NPC with control lay in complex-variable form.	40
2.13	Control block of inner loop in d -axis.	40
2.14	Control block of inner loop in q -axis.	40
2.15	Control block of inner loop in d - q -axis.	41
2.16	Block diagram of equations 2.32 and 2.33 in d -axis.	41
2.17	Block diagram of equations 2.32 and 2.33 in q -axis.	41
2.18	Block diagram of equations 2.32 and 2.33 in d - q -axis, where $G_d(s) = 1$	41
2.19	Control block of inner loop in d - q -axis.	42
2.20	Control block of middle loop in d -axis.	43
2.21	Control block of middle loop in q -axis.	43
2.22	Control block of middle loop in d - q -axis.	43
2.23	Block diagram of equations 2.42 and 2.43 in d -axis.	43
2.24	Block diagram of equations 2.42 and 2.43 in q -axis.	44
2.25	Block diagram of equations 2.42 and 2.43 in d - q -axis.	44
2.26	Control block of middle loop in d - q -axis.	44
2.27	Control block of outermost loop in d -axis.	45
2.28	Control block of outermost loop in q -axis.	46
2.29	Control block of outermost loop in d - q -axis.	46
2.30	Block diagram of equations 2.52 and 2.53 in d -axis.	46
2.31	Block diagram of equations 2.52 and 2.53 in q -axis.	46
2.32	Block diagram of equations 2.52 and 2.53 in d - q -axis.	46

2.33	Control block of outer loop in d - q -axis.	47
2.34	Block diagram of DC-bus capacitor voltage balancing controller.	48
2.35	Block diagram of NPC with its control.	50
2.36	Control block of inner loop in d -axis.	51
2.37	Control block of middle loop in d -axis.	52
2.38	Control block of outermost loop in d -axis.	52
3.1	Schematic diagram of grid-tied converter with LCL filter.	57
3.2	Equivalent circuit.	57
3.3	Block diagram of cascaded control for LCL filter in d - q coordinate system with an estimated algorithm based on sensing inverter side inductor current.	59
3.4	Grid integrated single stage solar photovoltaic system with NPC converter.	60
3.5	Equivalent circuit.	61
3.6	Block diagram of cascaded control for LCL filter in d - q coordinate system with an estimated algorithm based on sensing filter capacitor voltage.	65
3.7	Bode plots of the grid current loop (a) Bode diagrams for L_g from 0 mH to 5 mH, (b) Bode diagrams for L_1 from 2 mH to 3 mH, (c) Bode diagrams for C from 4 μ F to 6 μ F and (d) Bode diagrams for time delay variation.	66
3.8	Pole-zero map of TLC with (a) Sensing i_g , (b) Sensing i_i and (c) Bode plot of TLC with (1) Sensing i_g and (2) Sensing i_i	70
3.9	Block diagram of single current sensor based three-loop control scheme for LCL filter-based grid-tied converter.	72
3.10	Schematic diagram of grid connected converter with LCL filter.	73
3.11	Single-phase equivalent circuit.	73
3.12	Block diagram of control loop model in d -axis.	74
3.13	Block diagram of single current sensor based three-loop control scheme for LCL filter-based grid-tied converter.	76
3.14	Phasor diagram for evaluation of β phase grid current.	79
3.15	Simulated response of current/voltage dq component (a) Measured and estimated v_{cd} , v_{cq} , i_{gd} and i_{gq} , (b) Reference and estimated i_{gd} and i_{gq} , (c) Reference and estimated v_{cd} and v_{cq} and (d) Reference and measured i_{id} and i_{iq}	81
3.16	(a) Harmonic spectrum of i_g , the performance of i_g for varying grid inductance, (b) L_g from 0 mH to 5 mH at 0.5 s, (c) L_g from 0 mH to 12.5 mH at 0.5 s, performance for varying delay time $T_s/2$ and $2T_s$, (d) TLC with sensing i_g and (e) TLC with sensing i_i	82

3.17	Waveform of i_g for different LCL -filter parameter value listed in Table 3.2.	83
3.18	Waveform of i_g for $L_1 / L_2(mH) = 2.33/0.045$ and $C = 15\mu F$.	83
3.19	Waveform of i_g for $L_1 / L_2(mH) = 1/0.3$ and $C = 20\mu F$.	83
3.20	Simulation results (a) Waveform of v_{ab} , voltage across capacitor (v_{dc1}, v_{dc2}), and grid current (i_g), (b) Waveform of v_{pcc} , i_i , and i_g , (c) Harmonic spectrum of i_g and (d) Measured and estimated i_{id} and i_{iq} , measured and estimated i_{gd} and i_{gq} .	84
3.21	Simulation results (a) Reference and estimated i_{gd} and i_{gq} , (b) Reference and measured v_{cd} and v_{cq} and (c) Reference and estimated i_{id} and i_{iq} .	85
3.22	Simulation results (a) Waveform of v_{pcc} and i_g for variation of L_1 from 2 mH to 3 mH, (b) Waveform of v_{pcc} and i_g for variation of C from 4 μF to 6 μF and (c) Waveform of i_{gd} and i_g for variation of L_g from 0 mH to 5 mH.	85
3.23	Simulation results waveform of i_{ga} for variation of T_d from $T_s/2$ to $2T_s$.	85
3.24	Simulation waveform of (a) Measured and estimated β phase grid current and (b) Harmonic spectrum of i_g .	87
3.25	Simulation waveform of change in active power (a) Reference and estimated i_{gd} , (b) Reference and estimated i_{gq} , (c) Reference and estimated v_{cd} , (d) Reference and estimated v_{cq} , (e) Reference and estimated i_{id} and (f) Reference and estimated i_{iq} .	87
3.26	Simulation waveform of change in active power (a) Grid side inductor current, (b) Filter capacitor voltage, (c) Inverter side inductor current and (d) Grid voltage and grid current.	88
3.27	Experimental result (a) Estimated and measured v_{cd} and v_{cq} and (b) Estimated and measured i_{gd} and i_{gq} .	88
3.28	Experimental result (a) v_{pcc}, i_i, i_g , (b) Reference and estimated i_{gd} and i_{gq} , (c) Reference and estimated v_{cd} and v_{cq} and (d) Reference and measured i_{id} and i_{iq} .	88
3.29	THD of i_g .	89
3.30	Experimental result with reactive power (a) Reference and estimated i_{gd} and i_{gq} , (b) Reference and estimated v_{cd} and v_{cq} , (c) Reference and measured i_{id} and i_{iq} , (d) v_{pcc}, i_i, i_g and (e) Active and reactive power of the system.	89
3.31	Experimental result: S: change indicator. Performance of i_g for varying (a) L_1 from 2 mH to 3 mH, (b) C from 4 μF to 6 μF and (c) L_2 from 2 mH to 3 mH.	90
3.32	Experimental result S: change indicator. Performance of i_g for varying (a) L_g from 0 mH to 5 mH, (b) L_g from 0 mH to 7.5 mH and (c) T_d for $T_s/2$ and $2T_s$.	90
3.33	Experimental results v_{ab} , voltage across capacitor (v_{dc1}, v_{dc2}), and grid current (i_g).	91

3.34	Experimental results (a) Waveform of v_{pcc} , i_i , and i_g , (b) Measured and estimated i_{id} and i_{iq} and (c) Measured and estimated i_{gd} and i_{gq}	92
3.35	Experimental results (a) Reference and estimated i_{gd} and i_{gq} , (b) Reference and measured v_{cd} and v_{cq} and (c) Reference and estimated i_{id} and i_{iq}	92
3.36	Experimental results (a) Waveform of v_{pcc} and i_g for variation of L_1 from 2 mH to 3 mH, (b) Waveform of v_{pcc} and i_g for variation of C from 4 μ F to 6 μ F and (c) Waveform of v_{pcc} and i_g for variation of L_g from 0mH to 5mH.	92
3.37	Experimental results waveform of i_g for variation of T_d from $T_s/2$ to $2T_s$	93
4.1	Schematic diagram of grid tied converter with LCL filter.	97
4.2	Block diagram of discrete modified dual SOGI based PLL [53].	100
4.3	Block diagram of modified SOGI in continuous domain [53].	101
4.4	Block diagram of discrete modified SOGI.	106
4.5	Trilateral control system diagram in d -axis.	107
4.6	Estimated algorithm-based trilateral control in positive d - q axis.	108
4.7	Estimated algorithm-based trilateral control in negative d - q axis.	110
4.8	Block diagram to obtain decoupled grid voltages.	112
4.9	Block diagram to obtain decoupled grid currents.	112
4.10	Block diagram of generating a gating signal for the implemented system.	115
4.11	Generation of voltage references.	120
4.12	Generation of gate pulses for NPC converter.	121
4.13	Phasor representation of current computation in β axis utilizing decoupled grid current component.	121
4.14	Block diagram of the grid current estimation in $\alpha - \beta$ axis utilizing decoupled grid current component.	122
4.15	System configuration.	123
4.16	Control algorithm for switching of VSI.	124
4.17	Structure of continuous SOGI.	126
4.18	Structure of discrete SOGI using IIR digital filter.	128
4.19	Structure of discrete DSOGI based PLL.	130
4.20	Structure of continuous SOGI.	131
4.21	Structure of discrete SOGI using IIR digital filter.	132
4.22	Simulated response (a) Steady-state performance of v_g , i_i , and i_g and (b) Harmonic spectrum of i_g	134

4.23	Simulated response (a) Dynamic-state performance of v_g , i_{ia} , and i_{ga} and (b) Dynamic-state performance of measured and estimated grid current.	135
4.24	Simulated response in weak grid (a) Waveform of v_g , i_i , and i_g for voltage rise in phase 'a' of grid voltage, (b) Waveform of v_g , i_i , and i_g for voltage drop in phase 'a' of grid voltage and (c) Waveform of v_g , i_i , and i_g for distorted voltage drop in phase 'a' of grid voltage.	136
4.25	Steady-state performance of the system (a) v_{gabc} , i_{gabc} , i_{labc} , and i_{iabc} , (b) Harmonic spectrum of i_g , (c) Harmonic spectrum of i_l and (d) Harmonic spectrum of i_i	137
4.26	Dynamic-performance of the system (a) v_{ga} , i_{ga} , i_{ia} , and i_{la} in case of load unbalance, (b) v_{gb} , i_{gb} , i_{ib} , and i_{lb} in case of load unbalance, (c) v_{dc} , v_{pv} , i_{pv} , and i_{ga} in case of solar irradiance variation, (d) v_g , i_g in case of unbalance grid voltage, (e) v_{ga} , i_{ga} , i_{ia} , and i_{la} in case of the grid under voltage and (f) v_{ga} , i_{ga} , i_{ia} , and i_{la} in case of grid over voltage.	138
4.27	(a) Comparison of implemented discrete SOGI control algorithm with conventional control algorithm and (b) Comparison of implemented discrete DSOGI PLL with conventional PLL.	139
4.28	Experimental result (a) Steady-state waveform of v_{ga} , i_{ia} , and i_{ga} and (b) Harmonic spectrum of i_g	140
4.29	Experimental result (a) Transient-state waveform of sensed and computed grid current (i_g) in $\alpha - \beta$ axis and (b) v_{ga} and i_{ga}	141
4.30	Experimental result in the weak grid (a) Waveform of v_g and i_g for voltage rise in one phase, (b) Waveform of v_g and i_g for voltage dip in one phase, (c) Waveform of v_g and i_g for voltage distorted in one phase and (d) Waveform of v_g and i_g for distorted voltage dip in one phase.	141
4.31	Comparative behavior of proposed PLL with existing PLL.	142
5.1	Grid integrated single stage solar PV system with NPC Converter.	146
5.2	ESR of (a) Electrolytic capacitor (b) Film capacitor.	149
5.3	FFT based thermal modelling of the DC-link capacitor.	150
5.4	Frequency factor of permissible ripple current I_{ac} versus frequency f.	151
5.5	Properties of electrolytic capacitor.	151
5.6	(a) Life expectancy of EPCOS electrolytic capacitor of B43712. (b) Life expectancy of KEMET film capacitor.	151
5.7	Unreliability of Al-capacitor and film capacitor.	153
5.8	Diagram of total cost of system.	153
5.9	Computation of duty cycle d_{i0} (a) Case I: $v_{ip} > v_{in}^{+1}$ and (b) Case II: $v_{ip} < v_{in}^{+1}$	157
5.10	Voltage reference generation.	159

5.11	Switching of NPC converter.	160
5.12	Modified phase signal A (a) Simulation waveform and (b) Experimental waveform.	161
5.13	Block diagram of DC-bus capacitor voltage balancing controller.	162
5.14	Block diagram in d - q coordinate system of current controller.	163
5.15	Block diagram in d - q coordinate system of DC-bus voltage controller.	163
5.16	Simulation waveform (C_{dc} is 40 μ F film capacitor) (a) (e_a) and (i_a, i_b, i_c) and (b) (v_{dc1}, v_{dc2}), (v_{ab}), and (i_a).	164
5.17	Simulation waveform (C_{dc} is 40 μ F film capacitor) (a) (v_{dc}), (P_{pv}), and (i_a) for abrupt solar radiation change, (b) (v_{dc}) and (v_{dc1}, v_{dc2}), (c) (v_{dc}), (v_{dc1}, v_{dc2}), and (i_a) when PV array is turned off and (d) (v_{dc}), (v_{dc1}, v_{dc2}), and (i_a) when PV array is turned on.	165
5.18	Simulation waveform DC-bus voltage and capacitor current for (a) $C_{dc} = 40$ μ F and (b) $C_{dc} = 3300$ μ F.	166
5.19	FFT of i_g : THD for C_{dc} (a) 3300 μ F and (b) 40 μ F.	166
5.20	Experimental waveform (C_{dc} is 40 μ F film capacitor) (a) (e_a), (i_a, i_b, i_c) of the PV system and (b) (v_{ab}), (i_a), and (v_{dc1}, v_{dc2}).	166
5.21	Experimental waveform (C_{dc} is 40 μ F film capacitor) (a) (v_{dc}), (P_{pv}), and (i_a) for abrupt solar radiation change, (b) (v_{dc}) and (v_{dc1}, v_{dc2}), (c) (v_{dc}), (v_{dc1}, v_{dc2}), and (i_a) when PV array is turned off and (d) (v_{dc}), (v_{dc1}, v_{dc2}), and (i_a) when PV array is turned on.	167
5.22	Experimental waveform of (e_a), (i_a, i_b, i_c) for (a) Voltage dip (sag), (b) Voltage rise (swell) and (c) (v_{an}), (i_a, i_b, i_c) under perturbation in load.	168
5.23	Experimental waveform of DC-bus voltage and capacitor current for (a) $C_{dc} = 40$ μ F and (b) $C_{dc} = 3300$ μ F.	168
A.1	Neutral point clamped converter.	179
A.2	T-type converter.	180
A.3	Conduction path of NPC Converter (a) State P ($I_{out} = +ve, V_{out} = +V_{dc}/2$), (b) State O ($I_{out} = +ve, V_{out} = 0$), (c) State N ($I_{out} = -ve, V_{out} = -V_{dc}/2$) and (d) State O ($I_{out} = -ve, V_{out} = 0$).	180
A.4	Conduction path of T-type Converter (a) State P ($I_{out} = +ve, V_{out} = +V_{dc}/2$), (b) State O ($I_{out} = +ve, V_{out} = 0$), (c) State N ($I_{out} = -ve, V_{out} = -V_{dc}/2$) and (d) State O ($I_{out} = -ve, V_{out} = 0$).	181
A.5	(a) Efficiency vs. Power for NPC and (b) Efficiency comparison of three-level converter based on silicon device with $\phi = 0^\circ$	185

A.6	Efficiency comparison of three-level converter (a) Based on silicon carbide device with $\phi = 0^\circ$, (b) Based on silicon carbide device with $\phi = 30^\circ$ and (c) Based on silicon, silicon carbide, and gallium nitride.	186
A.7	Loss breakdown analysis for NPC with different devices (a) SK30MLI066P (Si), (b) SCT3060AL (SiC) and (c) TP65H035 (GaN).	187
A.8	Loss breakdown analysis for T-Type (a) IKW20N60H3, IRG4PH40UDPbF (Si) and (b) SCT3060AL, SCT2080KE (SiC).	188
B.1	Design of inverter.	189
B.2	Experimental set-up.	192

List of Tables

2.1	Value of <i>LCL</i> -Filter Parameters for Different Rating of the System	29
2.2	Value of <i>LCL</i> -Filter Parameters for Same Rating of the System	30
2.3	<i>PI</i> Controller Gains	53
3.1	Stability Margin of TLC with Different Estimation Schemes	71
3.2	Comparative Performance of Different Values of <i>LCL</i> Filter	84
5.1	Parameter of capacitor for life time model	149
5.2	Comparison of Power Losses in Different Capacitors	151
5.3	Failure rate of each component of inverter system	155
5.4	Net Cost of Inverter Based on Different Capacitor for 15 Years	155
5.5	Net Cost of Inverter Based on Different Capacitor for 30 Years	155
5.6	Comparison of THD & V_{ripple}	169
5.7	Comparison of Loss, Cost & Lifetime Expectancy	169
5.8	Losses in Inverter for Different <i>PI</i>	169
A.1	Power Losses Simulation and Calculation Results for NPC and T-Type Converter with Different Devices	184
A.2	System Specifications	184
B.1	List of Components Used in Design of Inverter	191
C.1	System Parameter	193
C.2	Voltage Parameter	193
C.3	Voltage Parameter	193
C.4	Controller parameter	194
C.5	Parameters of the System	194
C.6	Controller Parameter in Weak Grid	194
C.7	Parameters of the System	195

Abbreviations

AC	Alternating Current
ANF	Adaptive Notch Filter
CDF	Cumulative Density Function
CHB	Cascaded H-Bridge
DC	Direct Current
DSOGI	Dual Second Order Generalized Integrator
DSP	Digital Signal Processor
EA-P&O	Enhanced Adaptive Perturb and Observation
EPLL	Enhanced Phase-Locked Loop
ESR	Equivalent Series Resistance
FFT	Fast Fourier Transform
GaN	Gallium Nitride
GPIO	General Purpose Input Output
IGBT	Insulated-gate bipolar transistor
IIR	Infinite Impulse Response
KCL	Kirchhoff's Current Law
KVL	Kirchhoff's Voltage Law
LF	Loop Filter
LPF	Low Pass Filter
M&R	Maintenance and Repair
M-DSOGI	Modified Dual Second Order Generalized Integrator
MNF-SOGI	Modified Notch Filter based Second-Order Generalized Integrator
MOSFET	Metal Oxide Semiconductor Field-Effect Transistor
MPPT	Maximum Power Point Tracking
MTTR	Mean Repair Time of the System
NF	Nyquist Frequency
NPC	Neutral Point Clamped Converter
OLTF	Open Loop Transfer Function
P&O	Perturb and Observe
PBC	Passivity-based Control
PCC	Point of Common Coupling
PD	Phase Detector
PLL	Phase Locked Loop
PV	Photo Voltaic

PWM	Pulse Width Modulation
RF	Resonant Frequency
RMS	Root Mean Square
Si	Silicon
SiC	Silicon Carbide
SOGI	Second Order Generalized Integrator
SPWM	Sinusoidal Pulse Width Modulation
SRF	Synchronous Reference Frame
SRF-PLL	Synchronous Reference Frame Phase Locked Loop
TF	Transfer Function
THD	Total Harmonic Distortion
TLC	Three Loop Control
UPS	Uninterrupted Power Supply
VCO	Voltage-Controlled Oscillator
VFI	Voltage-Fed Inverter
VSI	Voltage Source Inverter

Nomenclature

ω_c, ω_r	$2\pi f_c, 2\pi f_r$
C	LCL filter capacitance
C_b	Base LCL filter capacitance
C_{dc}	DC-link capacitance
C_{part}, C_{lt}	Replaced part cost and labor, including travel cost
$d_+ - q_+$	Positive d-q synchronous reference frame
$d_- - q_-$	Negative d-q synchronous reference frame
f_b	Bandwidth
f_g	Grid frequency
f_s, f_{sw}, T_s	Sampling frequency, switching frequency, sampling time
f_r, f_c	Resonance frequency, cut off frequency
f_{res}	Resonant frequency
$F(x)$	Weibull distribution's CDF
G_m, P_m	Gain margin, phase margin
$\hat{i}_{gde}, \hat{i}_{gqe}$	Estimated grid current in d and q axis
$\hat{i}_{ga}, \hat{i}_{gb}, \hat{i}_{gc}$	Grid currents
$\hat{i}_{gd}, \hat{i}_{gq}$	Grid currents in d and q axis
$\hat{i}_{gd*}, \hat{i}_{gde}, \hat{i}_{gq*}, \hat{i}_{gqe}$	Reference and estimated grid currents in d and q axis
$\hat{i}_{gm}, v_{cm}, \hat{i}_{im}$	Measured grid current, capacitor voltage, and inverter current
$\hat{i}_{gdm}, \hat{i}_{gqm}$	Measured grid current in d and q axis
$\hat{i}_{g\beta e}$	Estimated grid's current in a β axis
$\hat{i}_{ia}, \hat{i}_{ib}, \hat{i}_{ic}$	Inverter currents
$\hat{i}_{id*}, \hat{i}_{id}, \hat{i}_{iq*}, \hat{i}_{iq}$	Reference and measured inverter currents in d and q axis
$\hat{i}_{ide}, \hat{i}_{iqe}$	Estimated grid currents in d and q axis
$I_N, I_{c,rms}$	Grid phase current and rms of the DC-bus capacitor ripple current
k	Variable used for neutral point voltage controller
k_{max}, k_{min}	Reference signal for the upper carrier, and the lower carrier
k_{p1}, k_{i1}	PI of outer loop
k_{p2}, k_{i2}	PI of middle loop
k_{p3}, k_{i3}	PI of inner loop
L_{equ}, α	Equivalent inductance $L_1 + L_2, \frac{L_2}{L_1}$
L_{gmin}, L_{gmax}	Grid inductance minimum and maximum value
L_x, L_r	Time to failure in hour and time to failure at the rated voltage in hour
N_c, N	Number of components and number of years
PI_1, PI_2, PI_3	Outermost loop, middle loop, and innermost loop
P_r, P_D, P	The rated active power, power dissipation, and inverter output power
R_1, L_1	Inverter side resistance and inductance of LCL filter
R_2, L_2	Grid side resistance and inductance of LCL filter
R_g, L_g	Grid resistance and inductance
T_d	Delay time

T_a, T_h	Ambient temperature and hot spot temperature
v_{ao}, v_{bo}, v_{co}	Inverter terminal voltages
v_a, v_b, v_c	Phase inverter voltages
v_{ab}, v_{bc}, v_{ca}	Line to line inverter voltages
v_{cde}, v_{cqe}	Estimated capacitor voltage in d and q axis
$v_{cd*}, v_{cde}, v_{cq*}, v_{cqe}$	Reference and estimated capacitor voltages in d and q axis
v_{cdm}, v_{cqm}	Measured filter capacitor voltages in d and q axis
v_c, V_{gl-l}	Capacitor voltage and line-to-line grid voltage
v_{ca}, v_{cb}, v_{cc}	Capacitor voltages
v_{cd}, v_{cq}	Capacitor voltages in d and q axis
$v_{c(d_e)}, v_{c(q_e)}$	Estimated capacitor voltages in d and q axis
v_{dc1}, v_{dc2}	DC-link voltage across capacitors
v_{dc}	DC-link voltage
v_g, i_g	Grid voltage and grid current
v_{ga}, v_{gb}, v_{gc}	Grid voltages
v_i, i_i	Inverter voltage and grid current
v_{ia}, v_{ib}, v_{ic}	Inverter voltages
v_{id}, v_{iq}	Inverter output voltage in d and q axis
V_{out}, I_{out}	Inverter output voltage and current
$v_{pcca}, v_{pccb}, v_{pccc}$	Point of common coupling voltages in phase a,b,and c
v_{pccd}, v_{pccq}	Point of common coupling voltages in d and q axis
v_{pv}, i_{pv}, P_{pv}	PV voltage, current, and power
v_r, v_x, V_{ripple}	Rated voltage, used voltage, and ripple voltage
I_r, I_x	Ripple current, and applied ripple current
z_b, ϕ	Base impedance
ϕ	Phase delay of the grid current w.r.t the fundamental grid voltage